Available online at www.sciencedirect.com

ScienceDirect

Ceramics International 40 (2014) 4897–4902

CERAMICS INTERNATIONAL

www.elsevier.com/locate/ceramint

The effect of the crystallization of oxidation-derived SiO_2 on the properties of porous Si_3N_4–SiO_2 ceramics synthesized by oxidation

Xiangming Li, Pute Wu*, Delan Zhu

College of Water Resources and Architecture Engineering, Northwest A&F University, Yangling, Shaanxi 712100, PR China

Received 21 September 2013; received in revised form 11 October 2013; accepted 17 October 2013
Available online 25 October 2013

Abstract

The effect of the crystallization of oxidation-derived SiO_2 on the properties of porous Si_3N_4–SiO_2 ceramics synthesized by oxidation was studied over the range of oxidation temperature and time. The SiO_2 remains amorphous at the temperature lower than 1250 °C and starts to crystallize as the temperature rises to 1300 °C. At the temperature higher than 1300 °C, the crystallization of SiO_2 impacts greatly the flexural strength of porous Si_3N_4–SiO_2 ceramics. A rapid crystallization of SiO_2 at 1350 °C decreases the bonding strength of the necks between Si_3N_4 particles, leading to a serious decrease of flexural strength. An appropriate crystallization of SiO_2 at 1300 °C strengthens the bonding necks between Si_3N_4 particles. The porous Si_3N_4–SiO_2 ceramics oxidized at 1300 °C for 3 h show the highest flexural strength value of 82 MPa. The crystallization of SiO_2 has no effect on the dielectric property of porous Si_3N_4–SiO_2 ceramics. Porous Si_3N_4–SiO_2 ceramics demonstrate a low dielectric constant of 3.0–4.0 and dielectric loss of 3.0–4.0 $\times 10^{-3}$ due to their high total porosity and SiO_2 content.
© 2013 Elsevier Ltd and Techna Group S.r.l. All rights reserved.

Keywords: D. Si_3N_4; D. SiO_2; Crystallization; Flexural strength; Oxidation

1. Introduction

The radomes and antenna windows used on carrier rockets, airships, missiles and return satellites are made of excellent electromagnetic wave transparent materials with good mechanical and dielectric properties [1,2]. SiO_2 and Si_3N_4 are potential materials for fabricating electromagnetic wave transparent materials [3–5]. The dielectric constant of SiO_2 is smaller than 3.5, which satisfies the dielectric conditions of radomes and antenna windows [6,7], but the low flexural strength and poor shock resistance of SiO_2 are inadequate for advanced applications [8,9]. Si_3N_4 ceramics possess excellent mechanical properties [10–12], but their relatively high dielectric constant limits their functional applications [4,13,14].

Synthesizing porous Si_3N_4–SiO_2 ceramics is an effective approach to combine good mechanical properties of Si_3N_4 and good dielectric properties of SiO_2 [2,3,5,7], and meanwhile to overcome the drawbacks of SiO_2 and Si_3N_4. Oxidation sintering, carried out usually at 1200–1400 °C, is a usual method to synthesize porous Si_3N_4–SiO_2 ceramics. The effect of the oxidation temperature on the properties of porous Si_3N_4–SiO_2 ceramics has been studied [2,15]. During the oxidation process, the oxidation-derived SiO_2 is amorphous and begins to crystallize when temperature is higher than 1300 °C [15,16]. Too much cristobalite may deteriorate the mechanical properties of porous Si_3N_4–SiO_2 ceramics, so the suggested oxidation temperature is lower than 1300 °C [15]. However, the effect of the crystallization of SiO_2 on the properties of porous Si_3N_4–SiO_2 ceramics has not been clearly identified, and the optimal oxidation temperature and time for synthesizing porous Si_3N_4–SiO_2 ceramics has not been determined.

As revealed by our recent research, an appropriate crystallization of SiO_2, which occurs during the process of synthesizing porous Si_3N_4–SiO_2 ceramics, may increase the bonding strength of the necks between Si_3N_4 particles and increase the flexural strength of porous Si_3N_4–SiO_2 ceramics as a result. In the present paper, porous Si_3N_4–SiO_2 ceramics were synthesized by oxidation of Si_3N_4 preforms. The effect of the crystallization of oxidation-derived SiO_2 on the phase composition, Si_3N_4 oxidation ratio, volume shrinkage, total porosity, flexural strength,

*Corresponding author Tel.: +86 29 87092860; fax: +86 29 87012210.
E-mail address: gjzwpt@vip.sina.com (P. Wu).

0272-8842/$ - see front matter © 2013 Elsevier Ltd and Techna Group S.r.l. All rights reserved.
http://dx.doi.org/10.1016/j.ceramint.2013.10.072

microstructure and dielectric properties of porous Si_3N_4–SiO_2 ceramics were studied in detail, and the optimal oxidation temperature and time for synthesizing porous Si_3N_4–SiO_2 ceramics were discussed.

2. Experimental procedure

2.1. Preparation of porous Si_3N_4–SiO_2 ceramics

Si_3N_4 powder (α ratio > 90 wt%, β ratio < 10 wt%) was mixed with 5 wt% dextrin and 1 wt% carboxymethyl cellulose (CMC) in distilled water into slurry. The slurry was ball-milled for 20 h and dried for 10 h at 90 °C. The obtained powder blend was crushed and passed through a 120-mesh sieve, and then cold-pressed into cylindrical preforms of 30×50 mm^2 diameter by using a circular steel die. Finally, the preforms turned into porous Si_3N_4–SiO_2 ceramics by oxidizing in air at 1200–1350 °C for 1–5 h at a heating and cooling rate of 5 °C/min. During temperature rising stage, the preforms were protected by nitrogen.

2.2. Characterization and tests

The preforms were weighed before and after the oxidation process to calculate the oxidation ratio of Si_3N_4. The open porosity and bulk density were measured by the Archimedes method. The total porosity was calculated based on Si_3N_4 oxidation ratio, open porosity and bulk density of the porous Si_3N_4–SiO_2 ceramics. The shrinkage was estimated by measuring the dimensions of the preforms before and after the oxidation process. The phase analysis was conducted by X-ray diffraction (XRD). The microstructure was observed by scanning electron microscopy (SEM). The average value of the flexural strength was obtained by testing five specimens of $3 \times 4 \times 40$ mm^3.

The dielectric loss was measured at 14 GHz by a resonant cavity method using the $TE_{01\delta}$ mode [17]. During testing, the cylindrical specimens of 4×15 mm^2 diameter were placed on a 4 mm-high low dielectric loss sapphire spacer (dielectric constant 4.4, dielectric loss 1.5×10^{-5}) in a copper cavity with a silver coating. The surface resistance of the copper has been calculated from the Q of the TE_{011} resonance of the empty cavity to allow the results to be corrected for the loss from the cavity walls. The $TE_{01\delta}$ mode was examined using a vector network analyzer (Hewlett-Packard Hp8720ES) with 1 Hz resolution. The dielectric constant was measured the same way without the sapphire spacer and with the cavity height close to specimen thickness.

For the convenience of the following discussion, the porous Si_3N_4–SiO_2 ceramics oxidized at different temperatures for different times are named as SN–*m*–*n* (*m* stands for temperature, and *n* for time).

3. Results and discussion

The oxidation of Si_3N_4 takes place at the temperature higher than 900 °C [2] and starts from the surface of Si_3N_4 particles [15]. During the oxidation process at 1200–1350 °C, although dense SiO_2 coatings forms quickly around Si_3N_4 particles, oxygen could still diffuse through the coatings and react with Si_3N_4. As the temperature rises, the oxidation rate of Si_3N_4 becomes higher due to the increase of oxygen diffusion rate, and the oxidation-derived SiO_2 in porous Si_3N_4–SiO_2 ceramics show different phases. Fig. 1 shows the XRD patterns of Si_3N_4 raw powder and the porous Si_3N_4–SiO_2 ceramics oxidized at 1200–1350 °C for 3 h. As can be seen, SiO_2 remains amorphous at the temperature lower than 1250 °C, and the amount of amorphous SiO_2 increases gradually as the temperature rises from 1200 to 1250 °C. The crystallization of amorphous SiO_2 is a two-stage process, which includes nucleation (atomic rearrangement) and diffusion (crystal growth). The nucleation incubation period is long ($\tau = 5 \times 10^4$ s) [18,19], so the nucleation of cristobalite is theoretically difficult. Actually, amorphous SiO_2 starts to crystallize as soon as the temperature reaches to 1300 °C, and the nucleation of cristobalite is heterogeneous, which starts from the surface of SiO_2 and extends inwards [16,19–21]. Once nuclei generates, cristobalite will soon come into being from the rapid growing up of nuclei. As shown in Fig. 1, the cristobalite peak appears when temperature is 1300 °C and becomes strong as the temperature rises to 1350 °C, which means an extensive crystallization of SiO_2 occur.

Si_3N_4 raw powder is composed of α- and β-Si_3N_4 (Fig. 1), which are both hexagonal crystal structure with very similar atom arrangements [22], ABAB… stacking with continuous channels in the structure in the case of β-phase and ABCD… stacking without such channels in the case of α-Si_3N_4. This crystallographic difference gave rise to speculation on the better oxidation resistance of the α-Si_3N_4 [23,24]. As shown in Fig. 1, as the temperature rises, the peaks of β-Si_3N_4 decrease rapidly but the peaks of α-Si_3N_4 decrease slowly. Since the oxidation rate of β-Si_3N_4 is higher than that of α-Si_3N_4, the Si_3N_4 particles in the porous Si_3N_4–SiO_2 ceramics oxidized from the Si_3N_4 preforms with higher content of β-Si_3N_4 may be strongly bonded by more oxidation-derived SiO_2.

Fig. 2 shows the Si_3N_4 oxidation ratio of the porous Si_3N_4–SiO_2 ceramics oxidized at 1200–1350 °C for 3 h. As the temperature rises from 1200 to 1250 °C, the oxidation ratio of Si_3N_4 increases slightly from 35.6 to 38.7% because of the good sealing effect of dense SiO_2 coating around Si_3N_4 particles. As

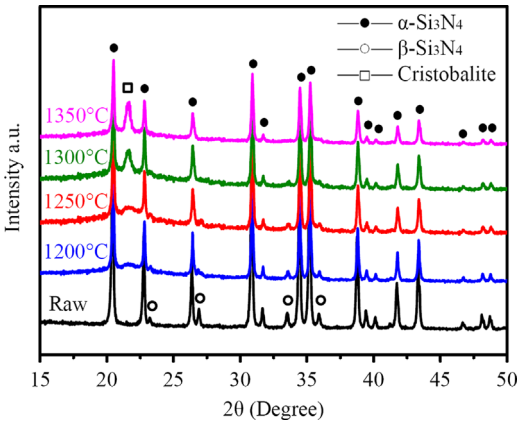

Fig. 1. XRD patterns of Si_3N_4 raw powder and the porous Si_3N_4–SiO_2 ceramics oxidized at 1200–1350 °C for 3 h.

the temperature rises to 1300 °C, SiO_2 starts to crystallize from the surface of SiO_2 coating [16,19–21], and cristobalite accumulates gradually at the surface of SiO_2 coating with oxidation time. The coefficient of thermal expansion (CTE) of cristobalite is 14.5×10^{-6}/°C [25], which is by far larger than that of Si_3N_4 (1.4×10^{-6}/°C) [5] and amorphous SiO_2 (0.5×10^{-6}/°C) [2]. Due to the CTE mismatch between cristobalite and amorphous SiO_2, there inevitably appear lots of microcracks at the surface of SiO_2 coating during the oxidation process. The microcracks provide channels for oxygen diffusion, so the oxidation ratio of Si_3N_4 increases obviously from 38.7 to 51.2% as the temperature rises from 1250 to 1350 °C.

Fig. 3 shows the volume shrinkage of porous Si_3N_4–SiO_2 ceramics as a function of oxidation time. At the beginning of the oxidation process, the oxidation-derived SiO_2 is in molten state [7,8], and the molten SiO_2 draws the Si_3N_4 particles closely with each other. With the increase of oxidation temperature and time, the drawing effect becomes obvious when more SiO_2 produces, resulting in an increase of volume shrinkage of porous Si_3N_4–SiO_2 ceramics. Taking the porous Si_3N_4–SiO_2 ceramics oxidized for 3 h as an example, the volume shrinkage increases from 1.7 to 3.7% as the temperature rises from 1200 to 1350 °C. Taking the porous Si_3N_4–SiO_2 ceramics oxidized at 1250 °C as another example, the volume shrinkage increases gradually from 1.6 to 2.7% with the increase of oxidation time from 1 to 5 h.

At the temperature higher than 1300 °C, the volume shrinkage of porous Si_3N_4–SiO_2 ceramics is co-affected by the oxidation ratio of Si_3N_4 and the crystallization of oxidation-derived SiO_2. Taking the porous Si_3N_4–SiO_2 ceramics oxidized at 1350 °C as an example, at the beginning of the oxidation process, Si_3N_4 particles are drawn closely with each other by SiO_2, so the volume shrinkage increases from 2.5 to 3.7% with the increase of oxidation time from 1 to 3 h. As time increases to 3 h, a large amount of cristobalite accumulates at the surface of SiO_2 coating and forms rigid crusts around SiO_2 coating. As a result, the drawing effect of molten SiO_2 is restricted seriously by rigid cristobalite crusts. In addition, as oxidation time increases further, the volume of rigid cristobalite crusts expands gradually because the oxidation of Si_3N_4 is a volume expansion process. Due to above two reasons, the volume shrinkage of the porous Si_3N_4–SiO_2 ceramics oxidized at 1350 °C decreases on the contrary from 3.7 to 3.5% as oxidation time increases from 3 to 5 h.

Fig. 4 shows the total porosity of porous Si_3N_4–SiO_2 ceramics as a function of oxidation time. Generally, the total porosity of porous Si_3N_4–SiO_2 ceramics decreases with the increase of oxidation temperature and time, and the variations of Si_3N_4 oxidation ratio and volume shrinkage have strong impacts on total porosity. Because of the gradual increase of Si_3N_4 oxidation ratio and volume shrinkage, the total porosity of the porous Si_3N_4–SiO_2 ceramics oxidized at the temperature lower than 1250 °C decreases slowly with oxidation time. Taking the porous Si_3N_4–SiO_2 ceramics oxidized at 1250 °C as an example, the total porosity decreases from 45.6 to 36.6% with the increase of oxidation time from 1 to 5 h. When temperature is higher than 1300 °C, Si_3N_4 oxidation ratio and volume shrinkage of porous Si_3N_4–SiO_2 ceramics increase with oxidation time, and therefore the total porosity of porous Si_3N_4–SiO_2 ceramics decrease rapidly. As oxidation time increases further, the total porosity decreases slowly due to the decreases of volume shrinkage. Taking the porous Si_3N_4–SiO_2 ceramics oxidized at 1350 °C as an example, the total porosity decreases rapidly from 40.5 to 29.6% as oxidation

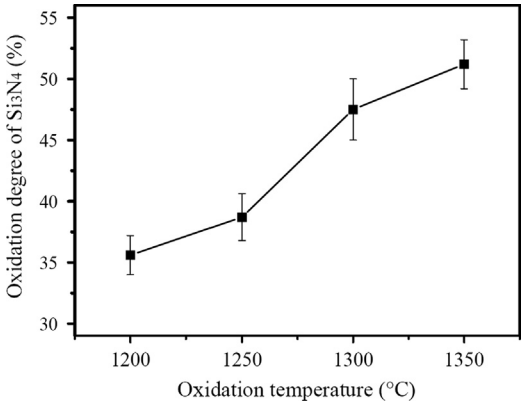

Fig. 2. Si_3N_4 oxidation ratio of the porous Si_3N_4–SiO_2 ceramics oxidized at 1200–1350 °C for 3 h.

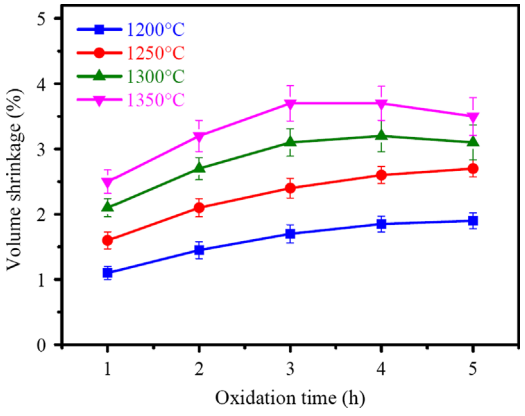

Fig. 3. Volume shrinkage of porous Si_3N_4–SiO_2 ceramics as a function of oxidation time.

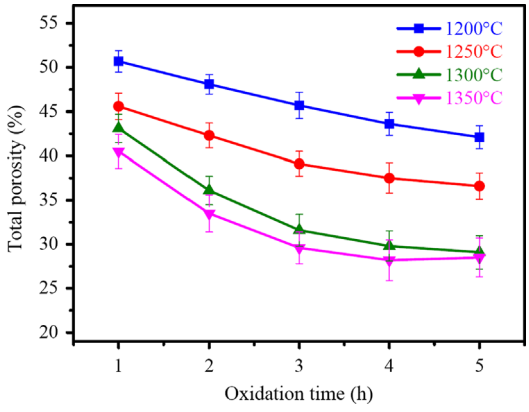

Fig. 4. Total porosity of porous Si_3N_4–SiO_2 ceramics as a function of oxidation time.

time increases from 1 to 3 h. However, it remains almost unchanged with the increase of oxidation time from 3 to 5 h.

Fig. 5 shows the flexural strength of porous Si_3N_4–SiO_2 ceramics as a function of oxidation time. SiO_2 remains amorphous during the oxidation process at the temperature lower than 1250 °C, and therefore the flexural strength of porous Si_3N_4–SiO_2 ceramics is co-affected by Si_3N_4 oxidation ratio and total porosity. During the oxidation process, Si_3N_4 particles are bonded by SiO_2, and the bonding strength of the necks between Si_3N_4 particles is the key factor affecting the flexural strength of porous Si_3N_4–SiO_2 ceramics. The bonding necks become strong with the increase of SiO_2, so the flexural strength of porous Si_3N_4–SiO_2 ceramics increases with oxidation time. As shown in Fig. 5, as oxidation time increases from 1 to 5 h, the flexural strength of the porous Si_3N_4–SiO_2 ceramics oxidized at 1250 °C increases from 20 to 54 MPa.

At the temperature higher than 1300 °C, the crystallization rate of SiO_2 increases gradually with the increase of oxidation temperature and time. Now, the flexural strength of porous Si_3N_4–SiO_2 ceramics is co-affected mainly by Si_3N_4 oxidation ratio and crystallization rate of SiO_2. The flexural strength of the porous Si_3N_4–SiO_2 ceramics oxidized at 1300 °C increases rapidly from 44 to 82 MPa with the increase of oxidation time from 1 to 3 h due to the increase of Si_3N_4 oxidation ratio. The crystallization of SiO_2 is a negative factor that decreases the bonding strength of the necks between Si_3N_4 particles [15]. As oxidation time increases from 3 to 5 h, although the bonding necks become thicker with the increase of Si_3N_4 oxidation ratio, the bonding strength of the necks actually decreases because of the large cristobalite generation at the surface of SiO_2. Therefore, the flexural strength of porous Si_3N_4–SiO_2 ceramics decreases on the contrary from 82 to 62 MPa. At 1350 °C, the negative effect of SiO_2 crystallization on the flexural strength of porous Si_3N_4–SiO_2 ceramics occurs earlier and more obviously. As shown in Fig. 5, the flexural strength of the porous Si_3N_4–SiO_2 ceramics oxidized at 1350 °C reaches to the highest value of 63 MPa when oxidation time is 2 h, and then decreases rapidly to 38 MPa as oxidation time increases to 5 h.

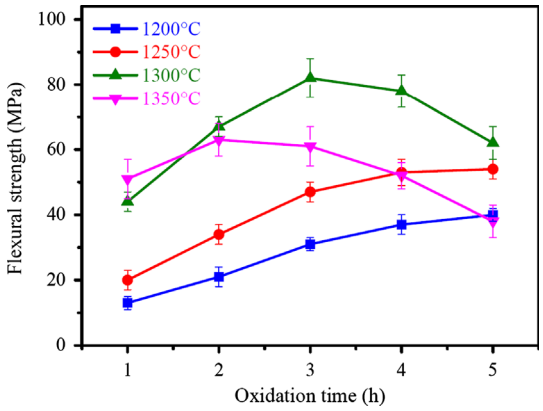

Fig. 5. Flexural strength of porous Si_3N_4–SiO_2 ceramics as a function of oxidation time.

From the results shown in Fig. 5, the optimal oxidation time for synthesizing porous Si_3N_4–SiO_2 ceramics is 5 h at the temperature lower than 1250 °C, 3 h at 1300 °C and 2 h at 1350 °C. Fig. 6 compares the SEM micrographs of SN–*m*1200–*n*5, SN–*m*1250–*n*5, SN–*m*1300–*n*3 and SN–*m*1350–*n*2. As shown in Fig. 6, the size of Si_3N_4 particles increases gradually as the temperature rises because of the stronger drawing of SiO_2. The porous Si_3N_4–SiO_2 ceramics oxidized at 1300 °C for 3 h show the most uniform microstructure and have the strongest bonding necks between Si_3N_4 particles and micro-sized pores among Si_3N_4 particles. Due to above reasons, the porous Si_3N_4–SiO_2 ceramics oxidized at 1300 °C for 3 h certainly possess the highest flexural strength, which is consistent with the results shown in Fig. 5.

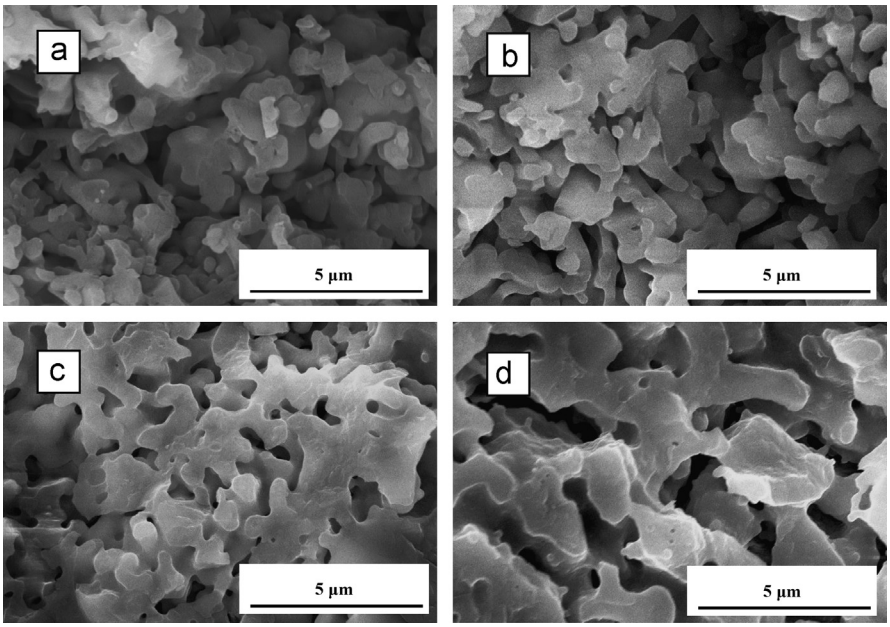

Fig. 6. SEM micrographs of (a) SN–*m*1200–*n*5, (b) SN–*m*1250–*n*5, (c) SN–*m*1300–*n*3 and (d) SN–*m*1350–*n*2.

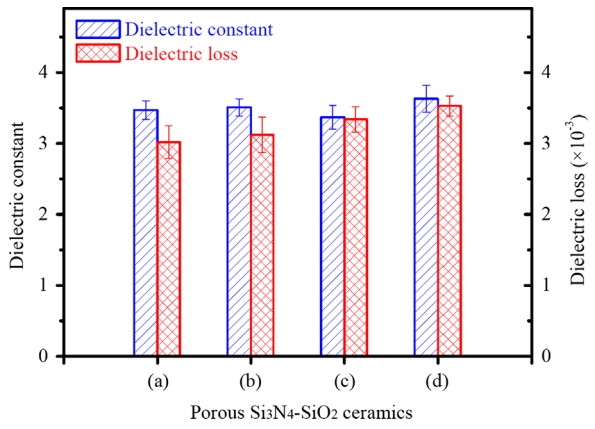

Fig. 7. Dielectric constant and loss of (a) SN–*m*1200–*n*5, (b) SN–*m*1250–*n*5, (c) SN–*m*1300–*n*3 and (d) SN–*m*1350–*n*2.

The dielectric constant of porous materials (ε') is lower than that of dense materials (ε). When $\varepsilon' \ll \varepsilon$, an approximation equation can be used to calculate ε', [27,28] as shown in

$$\varepsilon' = \varepsilon\left(1 - \frac{3P(\varepsilon-1)}{2\varepsilon+1}\right) \quad (1)$$

where P is the total porosity. As known from Eq. (1), the increase of total porosity leads to a smaller dielectric constant. Fig. 7 compares the dielectric constant and loss of SN–*m*1200–*n*5, SN–*m*1250–*n*5, SN–*m*1300–*n*3 and SN–*m*1350–*n*2. Among the four ceramics, SN–*m*1200–*n*5 has the highest total porosity while SN–*m*1300–*n*3 has the lowest one, so SN–*m*1200–*n*5 is supposed to possess a dielectric constant much lower than SN–*m*1300–*n*3 according to Eq. (1).

For a well-distributed two-phase composite, dielectric constant can be calculated according to Lichtencker's logarithmic equation [15]

$$Ln\varepsilon = v_1 Ln\varepsilon_1 + v_2 Ln\varepsilon_2 \quad (2)$$

where ε_1 and ε_2 are the dielectric constant of Si_3N_4 and SiO_2 respectively, v_1 and v_2 are the volume fraction of Si_3N_4 and SiO_2 respectively. The dielectric constant of SiO_2 (3.4) is much lower than that of Si_3N_4 (8.0), and the oxidation ratio of Si_3N_4 in SN–*m*1300–*n*3 is much higher than that in SN–*m*1200–*n*5. Therefore, though SN–*m*1300–*n*3 has a much lower total porosity than SN–*m*1200–*n*5, SN–*m*1300–*n*3 shows the lowest dielectric constant of 3.37 among the four ceramics shown in Fig. 7.

So far, some researches support the point that dielectric loss decreases with the increase of porosity. However, the dielectric loss of a material is co-affected by many factors [15,26–29]. As to the four porous Si_3N_4–SiO_2 ceramics shown in Fig. 6, the total porosity decreases in general and the oxidation ratio of Si_3N_4 increases as the temperature rises from 1200 to 1350 °C. The dielectric loss of SiO_2 is about 0.4×10^{-3} which is much lower than that of Si_3N_4 (2.0×10^{-3}) [2]. Therefore, co-affected by the variations of total porosity and oxidation ratio of Si_3N_4, the four porous Si_3N_4–SiO_2 ceramics show irregular dielectric loss. Due to the high total porosity and SiO_2 content, the four porous Si_3N_4–SiO_2 ceramics demonstrate low dielectric loss in the range of $3.0–4.0 \times 10^{-3}$.

4. Conclusions

The effect of the crystallization of oxidation-derived SiO_2 on the mechanical and dielectric properties of porous Si_3N_4–SiO_2 ceramics was studied in detail. At the temperature lower than 1250 °C, SiO_2 remains amorphous during the oxidation process, the flexural strength of porous Si_3N_4–SiO_2 ceramics increases slowly with oxidation time due to the gradual strengthening of bonding necks between Si_3N_4 particles. At the temperature higher than 1300 °C, the crystallization of SiO_2 has a big impact on the flexural strength of porous Si_3N_4–SiO_2 ceramics. An appropriate crystallization of SiO_2 at 1300 °C strengthens the bonding necks between Si_3N_4 particles, and therefore increases the flexural strength of porous Si_3N_4–SiO_2 ceramics positively. A rapid crystallization of SiO_2 at 1350 °C decreases the bonding strength of the necks between Si_3N_4 particles, leading to a serious decrease of the flexural strength of porous Si_3N_4–SiO_2 ceramics. The dielectric property of porous Si_3N_4–SiO_2 ceramics has nothing to do with the crystallization of SiO_2. Porous Si_3N_4–SiO_2 ceramics demonstrate low dielectric loss in the range of $3.0–4.0 \times 10^{-3}$ due to their high total porosity and SiO_2 content.

Acknowledgments

The authors gratefully acknowledge the financial support from the National Natural Science Foundation of China (51209177) and the Special Financial Grant from the China Postdoctoral Science Foundation (2013T60891). This work was also supported by the Financial Grant for Science and Technology Young Star from Shaanxi Province (2013KJXX-14) and the Basic Research Fund of Northwest A&F University (QN2012024).

References

[1] X.M. Li, L.T. Zhang, X.W. Yin, Fabrication and properties of porous Si_3N_4 ceramic with high porosity, J. Mater. Sci. Technol. 28 (2012) 1151–1156.
[2] S.Q. Ding, Y.P. Zeng, D.L. Jiang, Oxidation bonding of porous silicon nitride ceramics with high strength and low dielectric constant, Mater. Lett. 61 (2007) 2277–2280.
[3] Z.L. Hou, L. Zhang, J. Yuan, W.L. Song, M.S. Cao, High-temperature dielectric response and multiscale mechanism of SiO_2/Si_3N_4 nanocomposites, Chin. Phys. Lett. 25 (2008) 2249–2252.
[4] J. Barta, M. Manela, R. Fischer, Si_3N_4 and Si_2N_2O for high performance radomes, Mater. Sci. Eng. 71 (1985) 265–272.
[5] J.D. Walton, Reaction sintered silicon nitride for high temperature radome applications, Am. Ceram. Soc. Bull. 53 (1974) 255–258.
[6] M.S. Cao, H.B. Jin, J.G. Li, L. Zhang, Q. Xu, X. Li, L.T. Xiong, Ablated transformation and dielectric of SiO_2/SiO_2 nanocomposites dipped with silicon resin, Key Eng. Mater. 336–338 (2007) 1239–1241.
[7] D.C. Jia, Y. Zhou, T.Q. Lei, Ambient and elevated temperature mechanical properties of hot-pressed fused silica matrix composite, J. Eur. Ceram. Soc. 23 (2003) 801–808.
[8] J.S. Lyons, T.L. Starr, Strength and toughness of slip-cast fused silica composites, J. Am. Ceram. Soc. 77 (1994) 1673–1675.
[9] C.M. Xu, S.W. Wang, X.X. Huang, J.K. Guo, Processing and properties of unidirectional SiO_2/SiO_2 composites, Ceram. Int. 33 (2007) 669–673.
[10] F.L. Riley, Silicon nitride and related materials, J. Am. Ceram. Soc. 83 (2000) 245–265.

[11] S.Q. Guo, N. Hirosaki, Y. Yamamoto, T. Nishimura, M. Mitomo, Hot-pressed silicon nitride ceramics with Lu_2O_3 additives: elastic moduli and fracture toughness, J. Eur. Ceram. Soc. 23 (2003) 537–545.
[12] H. Arik, Synthesis of Si_3N_4 by the carbothermal reduction and nitridation of diatomite, J. Eur. Ceram. Soc. 23 (2003) 2005–2014.
[13] C.R. Zou, C.R. Zhang, B. Li, S.Q. Wang, F. Cao, Microstructure and properties of porous silicon nitride ceramics prepared by gel-casting and gas pressure sintering, Mater. Des. 44 (2013) 114–118.
[14] F. Chen, F. Cao, H.L. Pan, K.Y. Wang, Q. Shen, J.L. Li, S.Q. Wang, Mechanical and dielectric properties of silicon nitride ceramics with high and hierarchical porosity, Mater. Des. 40 (2012) 562–566.
[15] X.M. Li, X.W. Yin, L.T. Zhang, L.F. Cheng, Y.C. Qi, Mechanical and dielectric properties of porous Si_3N_4–SiO_2 composite ceramics, Mater. Sci. Eng. A 500 (2009) 63–69.
[16] X.M. Li, X.W. Yin, L.T. Zhang, S.S. He, The devitrification kinetics of silica powder heat-treated in different conditions, J. Non-Cryst. Solids 354 (2008) 3254–3259.
[17] M.S. Cao, Z.L. Hou, X.L. Shi, F.C. Wang, A research on high-temperature permittivity and loss tangent of low-loss dielectric by resonant-cavity technique, High Technol. Lett. 13 (2007) 279–282.
[18] A. Marotta, A. Buri, F. Branda, S. Saiello, Nucleation and crystallization of $Li_2O \cdot 2SiO_2$: a DTA study, in: J.H. Simmons, D.R. Uhlmann, G.H. Beall (Eds.), Advances in Ceramics, Nucleation and Crystallization in Glasses, American Ceramic Society, Westerville OH, PA, 1982, pp. 146–152.
[19] A. Marotta, S. Saiello, F. Branda, A. Buri, Activation energy for the crystallization of glass from DDTA curves, J. Mater. Sci. 17 (1982) 105–108.
[20] F.E. Wagstaff, Crystallization and melting kinetics of cristobalite, J. Am. Ceram. Soc. 52 (1969) 650–654.
[21] F.E. Wagstaff, Crystallization kinetics of internally nucleated vitreous silica, J. Am. Ceram. Soc. 51 (1968) 449–452.
[22] R. Marchand, Y. Laurent, J. Lang, Structure du nitrure de silicium, Acta Crystallogr. B 25 (1969) 2157–2160.
[23] D.P. Butt, D. Albert, T.N. Taylor, Kinetics of thermal oxidation of silicon nitride powders, J. Am. Ceram. Soc. 79 (1996) 2809–2814.
[24] M. Backhaus-Ricoult, V. Guerin, A.M. Huntz, V.S. Urbanovich, High temperature oxidation behavior of high-purity α-, β-, and mixed silicon nitride ceramics, J. Am. Ceram. Soc. 85 (2002) 385–392.
[25] W.T. Sweeney, Cristobalite for dental investment, J. Am. Dent. Assoc. 20 (1933) 108–119.
[26] S.J. Penn, N.M. Alford, A. Templeton, X.R. Wang, M.S. Xu, M. Reece, K. Schrapel, Effect of porosity and grain size on the microwave dielectric properties of sintered alumina, J. Am. Ceram. Soc. 80 (1997) 1885–1888.
[27] C.T. Lee, C.Y. Huang, Y.C. Lin, J. Yang, Structural and dielectric characteristics in a $Ca(Mg_{1/3}Nb_{2/3})O_3$–$CaZrO_3$ system, J. Am. Ceram. Soc. 90 (2007) 3148–3155.
[28] E.S. Kim, K.H. Yoon, Effect of nickel on microwave dielectric properties of $BaMg_{1/3}Ta_{2/3}O_3$, J. Mater. Sci. 29 (1994) 830–834.
[29] I.T. Kim, Y.H. Kim, S.J. Chung, Order–disorder transition of microwave dielectric properties of $Ba(Ni_{1/3}Nb_{2/3})O_3$ ceramic, Jpn. J. Appl. Phys. 34 (1995) 4096–4103.